Nanomechanical resonators fabricated by atomic layer deposition on suspended 2D materials

Liu, H.; Basuvalingam, Saravana B.; Lodha, Saurabh; Bol, Ageeth A.; van der Zant, Herre S.J.; Steeneken, Peter G.; Verbiest, Gerard J.

DOI
10.1088/2053-1583/acf58a

Publication date
2023

Document Version
Final published version

Published in
2D Materials

Citation (APA)
Liu, H., Basuvalingam, S. B., Lodha, S., Bol, A. A., van der Zant, H. S. J., Steeneken, P. G., & Verbiest, G. J. (2023). Nanomechanical resonators fabricated by atomic layer deposition on suspended 2D materials. *2D Materials*, *10*(4), Article 045023. https://doi.org/10.1088/2053-1583/acf58a

Nanomechanical resonators fabricated by atomic layer deposition on suspended 2D materials

2D Materials

OPEN ACCESS

RECEIVED
9 May 2023

REVISED
17 August 2023

ACCEPTED FOR PUBLICATION
31 August 2023

PUBLISHED
8 September 2023

PAPER

Nanomechanical resonators fabricated by atomic layer deposition on suspended 2D materials

Hanqing Liu[1,*], Saravana B Basuvalingam[2], Saurabh Lodha[3], Ageeth A Bol[4], Herre S J van der Zant[5], Peter G Steeneken[1,5] and Gerard J Verbiest[1,*]

[1] Department of Precision and Microsystems Engineering, Delft University of Technology, Mekelweg 2, 2628 CD Delft, The Netherlands
[2] Department of Applied Physics, Eindhoven University of Technology, PO Box 513, 5600 MB Eindhoven, The Netherlands
[3] Department of Electrical Engineering, Indian Institute of Technology Bombay, 400076 Mumbai, India
[4] Department of Chemistry, University of Michigan, 930 N. University Ave., Ann Arbor, MI 48109, United States of America
[5] Kavli Institute of Nanoscience, Delft University of Technology, Lorentzweg 1, 2628 CJ Delft, The Netherlands
[*] Authors to whom any correspondence should be addressed.

E-mail: H.Liu-7@tudelft.nl and G.J.Verbiest@tudelft.nl

Keywords: nanomechanical resonator, atomic layer deposition, Q factor, resonance frequency, optomechanical drive

Supplementary material for this article is available online

Abstract

Atomic layer deposition (ALD), a layer-by-layer controlled method to synthesize ultrathin materials, provides various merits over other techniques such as precise thickness control, large area scalability and excellent conformality. Here we demonstrate the possibility of using ALD growth on top of suspended 2D materials to fabricate nanomechanical resonators. We fabricate ALD nanomechanical resonators consisting of a graphene/MoS_2 heterostructure. Using atomic force microscope indentation and optothermal drive, we measure their mechanical properties including Young's modulus, resonance frequency and quality factor, showing a lower energy dissipation compared to their exfoliated counterparts. We also demonstrate the fabrication of nanomechanical resonators by exfoliating an ALD grown NbS_2 layer. This study exemplifies the potential of ALD techniques to produce high-quality suspended nanomechanical membranes, providing a promising route towards high-volume fabrication of future multilayer nanodevices and nanoelectromechanical systems.

The properties of 2D materials, in particular their ultralow weight and ultrahigh mechanical flexibility, provides them with an excellent sensitivity to external forces [1–3]. Hence, resonators from 2D materials have become a popular choice for the next generation of nanoelectromechanical systems [4, 5]. Recently, there is surge towards stacking different 2D materials into heterostructures often exhibiting better sensing properties. Such heterostructures are used for tunable resonators and oscillators [6], and can potentially lead to better sensors in microphone and pressure sensing applications [5].

To achieve high-performance nanomechanical resonators, clean interfaces between different 2D materials are important [7]. Therefore, bottom-up synthesis methods were developed, of which chemical vapor deposition (CVD) is the most attractive due to its large-scale and high-quality growth. The main shortcoming of CVD, however, is the difficulty to accurately control the thickness and morphology of grown 2D materials. Atomic layer deposition (ALD), a vapor phase thin film deposition technique based on self-limiting surface reactions, inherently yields atomic-scale thickness control, excellent uniformity, and conformality [8]. ALD processes exists for a large variety of materials ranging from pure elements to metal oxides and chalcogenides [9]. In terms of 2D materials, ALD was applied to fabricate 2D-based field effect transistors, p–n diode devices, solar cells and photodetectors, displaying high electrical and optical uniformities [10]. Since experimental research of ALD materials for nanomechancial resonators is unexplored territory, it is of interest to study the potential of such devices and evaluate their mechanical performance.

In this work, we show two types of nanomechancial resonators fabricated using ALD: one consists of a heterostructure made from exfoliated graphene

(bottom layer) and ALD MoS_2 (top layer) and the other is ALD NbS_2. We use atomic force microscope (AFM) indentation to determine their Young's moduli and use an optomechanical method to study their resonance frequency and corresponding quality factor in vacuum conditions. The extracted parameters from our measurements agree well with literature values for 2D exfoliated or CVD resonators. Furthermore, by fitting a relation between the quality factors before and after ALD, we verify a low-level dissipation induced by ALD MoS_2. Our work indicates the potential of ALD fabrication techniques for realizing multilayer nanomechanical membranes and resonators with enhanced functionality and thickness control.

Results and discussion

The ALD layers are deposited (see figures 1(a) and (b)) by plasma-enhanced ALD (PE-ALD) technique using an Oxford Instruments Plasma Technology FlexAL ALD reactor. The base pressure of the system is 10^{-6} Torr. The metal-organic precursors bis(tert-butylimido)-bis(dimethylamido) molybdenum (STREM Chemical, Inc. 98%) and bis-tris-niobium are used for MoO_x and NbO_x growth, respectively [9, 11]. The Mo and Nb precursors are kept in stainless steel bubblers at 50 °C and 65 °C, respectively and are bubbled using Ar as the carrier gas. In both the processes, O_2 plasma is used as the coreactant. The MoO_x and NbO_x films are deposited at 100 °C and 150 °C, respectively. More details on the PE-ALD recipes can be found in supplementary S1.

Both the MoS_2 and NbS_2 films are synthesized by a two step approach. As the first step, metal oxide (MoO_x or NbO_x) film is deposited by PE-ALD technique. Next, the metal oxide film is sulfurized at 900 °C in H_2S environment (10% H_2S and 90% Ar) to form metal sulfide film (MoS_2 or NbS_2). As shown in figures 1(a) and (c), the MoS_2 film is synthesized by PE-ALD on top of suspended graphene drums, resulting in 10 resonators with a radius $r = 4\,\mu$m. Note that device D3 and D9 broke (buckled, figure 1(c)) during fabrication and will not be considered further. On the other hand, NbS_2 film is synthesized by growing NbO_x on glassy carbon followed by sulfurization at 900 °C. Then, we fabricate the NbS_2 resonators by transferring the NbS_2 films from glassy carbon substrate over circular cavities in a SiO_2/Si substrate to form suspended drums using the Scotch tape method [5] (see figure 1(b)). We tested the transfer of ALD nanoflakes with different thicknesses grown on different substrates and found that only the transfer of thick NbS2 films from glassy carbon to the substrate with cavities was possible (see table SI). The cavities have a depth of 285 nm and were fabricated by reactive ion etching (see supplementary S1). The fabricated NbS_2 resonators, shown in figure 1(d), have a radius of $r = 4\,\mu$m (devices D1 and D2) or $r = 3\,\mu$m (devices D4 and D5). We use AFM (tapping mode) to scan the surface of our fabricated samples, to determine the thickness of the 2D materials. By calculating the height difference between the membranes and substrate (see the statistics in figures 1(e) and (f)), we extract the mean thickness of the graphene $t_g = 13.3$ nm (40 layers), MoS_2 $t_m = 7.8$ nm (12 layers) and NbS_2 $t_n = 56.1$ nm (92 layers), respectively. The total thickness of the heterostructure is thus $t_h = t_m + t_g = 21.1$ nm.

Raman spectra of both ALD heterostructures and NbS_2 devices, obtained with a 515 nm green laser at room temperature (see supplementary S2), clearly show the expected Raman modes and thereby verify the quality of fabricated devices after the high-temperature ALD synthesis processes. We also measure and theoretically analyze the Raman intensity ratio between the Si peak of suspended MoS_2/graphene membrane and that of substrate (see figure S4), from which we conclude that ALD MoS_2 layer is only deposited on top (but not on bottom) of the exfoliated graphene membrane in the fabricated heterostructure devices.

After fabrication, we determine the Young's modulus of the ALD devices by indenting with an AFM (contact mode) cantilever at the center of the suspended area (see figure 2(a), insert). Following literature [12], the applied vertical force F versus membrane deflection δ for a circular membrane (composed of single material), as depicted in figure 2(a), is given by

$$F = \left(\frac{16\pi D}{r^2}\right)\delta + n_0\pi\delta + Etq^3\left(\frac{\delta^3}{r^2}\right), \qquad (1)$$

where $D = \gamma Et^3/(12(1-\nu^2))$ is bending rigidity, E is Young's modulus, ν is the Poisson ratio, n_0 is pretension, $q = 1/(1.05 - 0.15\nu - 0.16\nu^2)$, and γ is a factor that quantifies the effect of interlayer shear interactions on D in multilayer 2D materials [13]. The first two terms in equation (1) scale linearly with δ ($F \sim \delta$) and are set by D and n_0; while the third cubic term ($F \sim \delta^3$) is due to the geometric nonlinearity of the membrane, which lead to an increase in the in-plane stress that depends on its Young's modulus E. Note that equation (1) is suitable for NbS_2, while for heterostructures, it contains contributions from graphene and MoS_2 layers (see equation (S5)). We use the bulk Poisson ratios $\nu_g = 0.165$, $\nu_m = 0.25$ and $\nu_n = 0.28$ of graphene, MoS_2 and NbS_2, respectively, in further analysis. In addition, considering the measured layer numbers of graphene, MoS_2 and NbS_2 membranes, we use the factors $\gamma_g = 0.1$ and $\gamma_m = 0.4$ from literature [13] and assume $\gamma_n = \gamma_m$.

We extract E_h and E_n by the fitting the measured F versus δ with equations (S5) and (1), respectively, which nicely describe the experimental data for the NbS_2 device D1 (blue points) and the heterostructure

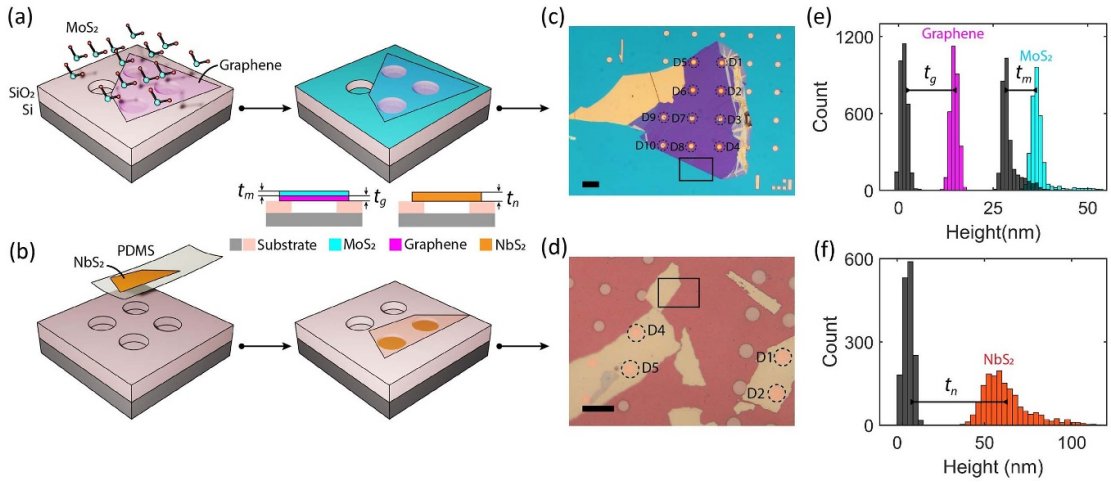

Figure 1. Fabrication of the ALD nanomechanical resonators measured in this work. (a) Fabrication process of exfoliated graphene/ALD MoS_2 heterostructure resonators. MoS_2 is directly deposited onto the suspended graphene membrane. (b) Fabrication process of ALD NbS_2 resonators. ALD NbS_2 flake is exfoliated from glassy carbon using PDMS, and then transferred on top of a prepatterned Si/SiO_2 substrate with circular cavities. Inserts between (a) and (b) are the cross-section views of the heterostructure and NbS_2 resonators, respectively. (c) and (d) Optical images of our fabricated heterostructure and NbS_2 devices, respectively, where the black scale bars are 20 μm. Note that the heterostructure devices D3 and D9 were broken during deposition. (e) and (f) Height histograms of SiO_2/Si substrate (black), graphene (carmine), MoS_2 (blue) and NbS_2 (orange) measured by AFM scanning, allow us to extract the thicknesses $t_g = 13.3$ nm, $t_m = 7.8$ nm, and $t_n = 56.1$ nm. The scanning areas for fixing t_g and t_n are the black frames in (c) and (d) respectively, while that for fixing t_m is the scratch on MoS_2 layer after deposition. We observe that the thickness distribution of ALD MoS_2 is satisfyingly as uniform as the exfoliated graphene, while the surface of thick ALD NbS_2 is rugged.

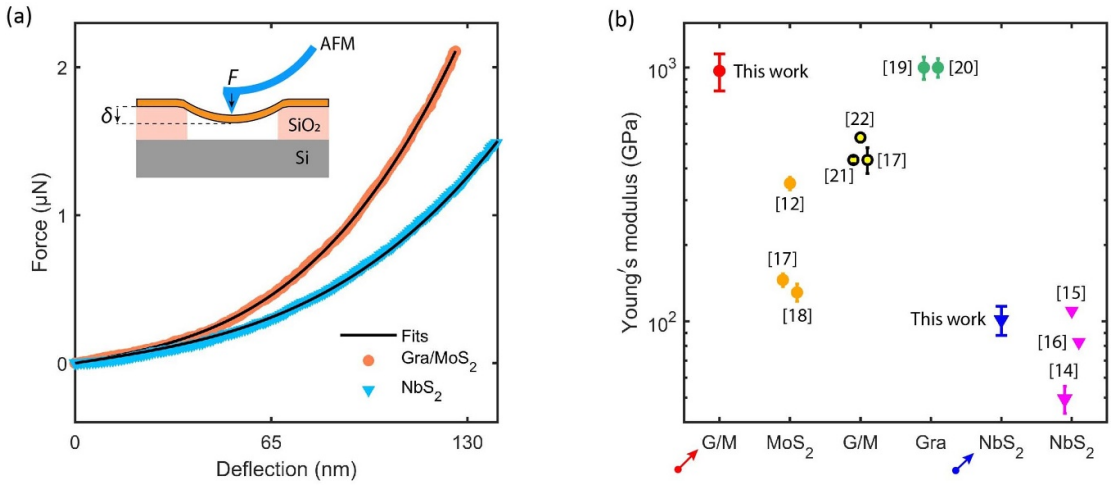

Figure 2. Static characterization of the fabricated ALD nanomechanical resonators. (a) Typical force-deflection curve obtained by AFM indentation onto the suspended part of heterostructure (orange points) and NbS_2 (blue points) resonators. The solid lines show fits using the model from equation (1), gives the pretension and Young's modulus of the membranes. Insert: schematic of AFM indentation. Statistics over all devices give the mean values of $E_h = 952$ GPa (heterostructure) and $E_n = 101$ GPa (NbS_2). (b) Comparison of Young's modulus between this work and previous studies. The numbers in brackets give the citations we select in (b).

device D2 (orange points) as shown in figure 2(a). The extracted statistics of effective Young's moduli for heterostructure devices (E_h) and Young's moduli (E_n) for NbS_2 devices give the mean values of $E_h = 952\pm 161$ GPa and $E_n = 101\pm 13$ GPa, respectively. In figure 2(b), we compare E_h and E_n with values reported in the literature: E_n shows a good agreement with the reported values of 75 ± 35 GPa [14–16]; E_h is between the reported values for MoS_2 250 ± 120 GPa and graphene membranes 1025 ± 125 GPa [12, 17–20], but higher than the reported values for similar fully exfoliated heterostructures 461 ± 43 GPa [17, 21, 22]. The larger E_h might be caused by the stronger interlayer adhesion or the larger intrinsic Young's modulus of ALD MoS_2. The standard deviations in extracted Young's moduli, ± 13 GPa and ± 161 GPa for NbS_2 and heterostructure resonators, respectively, are comparable to the ones reported in literature for exfoliated materials. This illustrates the high homogeneity of ALD materials.

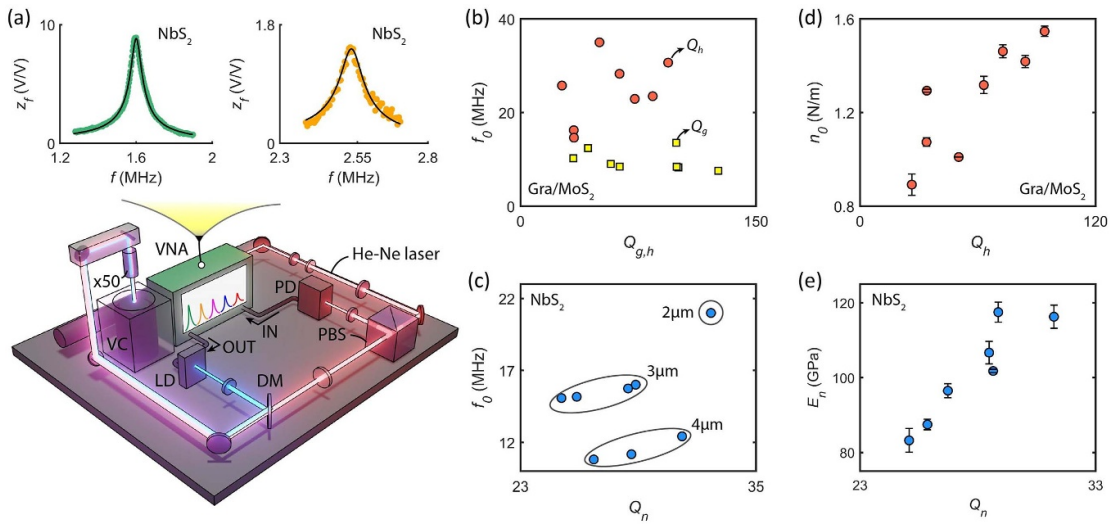

Figure 3. Dynamic characterization of the fabricated ALD nanomechanical resonators. (a) Top, the measured amplitude z_f (points) of NbS_2 device D6, around the fundamental and second resonance, respectively; z_f is fitted by a harmonic oscillator model (black lines) to extract resonance frequency and corresponding quality factor. Bottom, interferometry setup. ALD device is placed inside the vacuum chamber (VC). The diode laser (LD) is modulated by a vector network analyzer (VNA) to actuate the resonator, while intensity variations of the reflected He–Ne laser caused by resonator motion, are measured by photodiode (PD) and recorded with the VNA. PBS: polarized beam splitter; DM: dichroic mirror; x50: 50-fold objective. (b) The measured Q versus f_0 for graphene resonators before ALD (Q_g, yellow points) and for heterostructure resonators after ALD (Q_h, red points). (c) The measured Q_n versus f_0 for NbS_2 resonators. (d) Q_h versus the extracted pretension n_0. (e) Q_n versus the extracted Young's modulus E_n.

In addition to the Young's modulus, we also extract the pretension n_0 for each device. Supplementary tables SII and SIII show a complete overview of the obtained parameters from the fitting to equation (1). The extracted n_0 ranges from 0.45 to 1.55 N m^{-1} for all heterostructure and NbS_2 resonators, which are similar to values reported in the literature for resonators made by exfoliation and CVD [4, 21, 23].

Let us now focus on the dynamics of the ALD resonators. We measured the dynamic response of the membranes with a laser interferometer [23] (see figure 3(a), bottom). A power modulated blue diode laser ($\lambda = 405$ nm) photothermally actuates the resonator, while the refection of a continuous-wave red He–Ne laser ($\lambda = 632$ nm) is sensitive to the time-dependent position of membrane. A vector network analyzer (VNA) provides a signal at drive frequency f (OUT port) that modulates the blue laser intensity while the intensity of the red laser recorded by a fast photodiode is connected to the IN port. The VNA thus measures a signal z_f that is proportional to the ratio of the membrane amplitude and actuation force. By sweeping the drive frequency f, we locate the resonance peak in the range from 100 kHz to 100 MHz. Laser intensities are set to 0.3 mW (blue) and 1.1 mW (red), respectively. These intensities are low enough for the resonator to vibrate in the linear regime. All measurements were performed at room temperature in vacuum at a pressure of 10^{-5} mbar.

Figure 3(a) (top inserts) shows the measured signal z_f of NbS_2 device D6, at around the fundamental and second resonance frequency, respectively. By fitting z_f to the response function of a harmonic oscillator, we extract $f_0 = 16.0$ MHz with $Q = 28.9$ and $f_1 = 25.3$ MHz with $Q = 34.4$. For vibrations of clamped drums, we can compute the resonance frequencies f_i using [3]

$$f_i = \left(\frac{\mu_i}{2\pi}\right)\sqrt{\frac{D}{\sigma r^4}\left[\mu_i^2 + \frac{n_0 r^2}{D}\right]}, i = 0, 1, \ldots, \quad (2)$$

where $\sigma = \eta\rho t$ is the areal mass density, η is a correction factor of mass considering the contaminations on resonators, and μ_i is a mode-specific factor. We have $\mu_1 = 2.4048$ for the fundamental mode and $\mu_2 = 3.8317$ for the second mode. For an ideal membrane, in which $n_0 r^2$ is much larger than the flexural rigidity D and thus $n_0 r^2/D \to \infty$, we have $f_1/f_0 = \mu_1/\mu_0 = 1.59$; while for an ideal plate where D is much larger than $n_0 r^2$, we have $n_0 r^2/D \to 0$ and thus $f_1/f_0 = (\mu_1/\mu_0)^2 = 2.54$. The measured f_1/f_0 are 1.595 ± 0.167 and 1.959 ± 0.642 for heterostructure and NbS_2 devices, respectively (see supplementary tables SII and SIII), suggesting that the modes of heterostructure resonators are near the membrane limit, while the modes of NbS_2 resonators are in between the membrane and plate limit. We plot the extracted Q versus f_0 for all heterostructure resonators (Q_h) and NbS_2 resonators (Q_n) in figures 3(b) and (c), respectively, including the quality factor Q_g of the exfoliated graphene membranes before ALD. As expected from equation (2), f_0 decreases with increasing r for the NbS_2 resonators, while f_0^h for heterostructure resonators varies widely from 14.6 to 30.7 MHz. This is attributed to the inhomogenieties like wrinkles

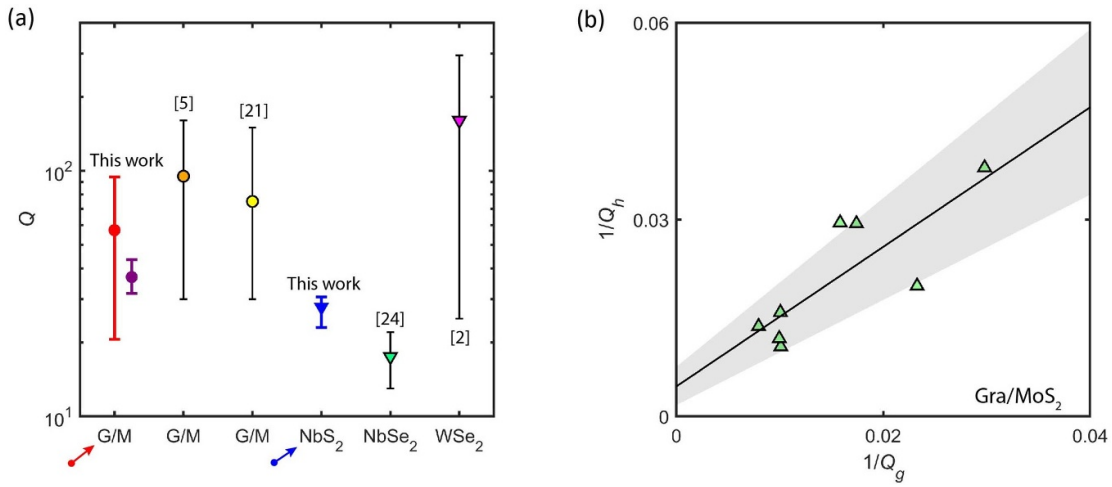

Figure 4. Energy dissipation in the fabricated ALD nanomechanical resonators. (a) Comparison of quality factor Q of 2D material resonators between this work and previous studies. Purple errorbar shows the measured Q of purely exfoliated heterostructure devices, as introduced in supplementary material. (b) The measured results of Q_h^{-1} versus Q_g^{-1} (green points) with a linear fit by equation (3) (black line). Gray shadow represents the fitting error bar.

and crumples in the heterostructures (see images in figure S5) and large differences in pretension. All measured resonance frequencies are comparable to those in literature reported for similar devices [3, 12].

The extracted values of Q_n and Q_h are also comparable to values of previously studied resonators made by exfoliation and CVD [2, 6, 21, 24], as illustrated in figure 4(a). To gain insight into the damping, we plot Q_h versus n_0 for heterostructure resonators and Q_n versus E_n for NbS_2 resonators, respectively, as plotted in figures 3(d) and (e). For both cases, we observe a linear relation, indicating that pretension plays a more important role on damping than bending rigidity for heterostructure resonators, while it is on the other way around for NbS_2 resonators. This is exactly as expected based on the ratio f_1/f_0. On the other hand, we do not see clear relations of Q_h versus E_h and Q_n versus n_0 as plotted in figures S6(a) and (b), respectively.

Concerning the effective masses, we determine the correction factors η_h and η_n by substituting the measured f_0, and the extracted n_0 and E into equation (2) (see values in supplementary tables I and II). We obtain $\eta_h = 1.34 \pm 0.92$ and $\eta_n = 2.87 \pm 0.83$, respectively. The high η_n of NbS_2 devices is attributed to the contaminations from the PDMS stamping. The values η_h for the heterostructure are surprisingly close or even below 1. This suggests the absence of any residues and possibly even the thinning of the graphene membrane during the ALD process, while the ALD MoS_2 layer is mainly deposited on top of the suspended graphene membrane instead of bottom (see supplementary S2).

We also observe a general decrease of quality factor in heterostructure resonators after ALD ($Q_h < Q_g$), as shown in figure 3(b). Considering the dissipation mechanism for two parallel membranes, the overall Q_h can be modeled as

$$1/Q_h = \alpha/Q_g + 1/Q_m, \tag{3}$$

where α can be different than 1 on account of structural changes in the graphene because of the ALD process, and Q_m^{-1} is a fit parameter that represents the damping in the heterostructure originating from the ALD MoS_2. We fit the measured Q_h^{-1} versus Q_g^{-1} with equation (3) (see figure 4(b)) and extract $\alpha = 1.1 \pm 0.1$ and $1/Q_m = 4.7 \pm 3.1 \times 10^{-3}$. The fact that the obtained α (within errors) is close to 1, provides evidence that there little to none increase of the dissipation in the graphene during the ALD process. A control experiment has been done with purely exfoliated graphene/MoS_2 heterostructures (see figure S7), giving us $\alpha = 1.1 \pm 0.2$ and $1/Q_m = 17.6 \times 10^{-3}$. The lower $1/Q_m$ of ALD heterostructure compared to exfoliated layers can be attributed to a better conformality of the ALD layer and the absence of contamination by transfer polymers.

Compared with PE-CVD method that grows 2D materials under a temperature more than 400 °C, the reaction temperature window for ALD here is much lower (100 °C for MoO_x deposition), which significantly improve the survival rate of suspended graphene membranes. Therefore, PE-ALD is a safer and more efficient method for fabricating high-performance 2D heterostructure resonators. In addition, although ALD is known to be capable of wafer-scale synthesis, the dimensions of our fabricated devices are still quite small due to the use of exfoliation in the fabricating process. A strategy could be to grow transfer less suspended CVD 2D material membranes like graphene [25], and subsequently grow ALD material

heterostructures from them. In addition, ALD could benefit from a method to precisely control the flatness, so as to avoid the cragged surfaces of nanoscale devices as illustrated in figures S5(a) and (b).

2. Conclusions

In conclusion, we presented the fabrication and mechanical characterization of nanomechanical resonators consisting of ALD 2D materials. We developed two PEALD based approaches to suspend ALD flakes on a patterned Si/SiO_2 substrate: one is dry transfer using PDMS (exfoliate ALD Nb_2 flakes from glassy carbon); the other is ALD deposition of MoS_2 on mechanically exfoliated suspended graphene drums. AFM indentation allows us to determine their Young's moduli as 101.4± 13.3 GPa and 951.7± 161.0,GPa. Using an optomechanical method, we extracted their resonance frequencies and the corresponding quality factors. All of the above parameters are well comparable to the reported values of exfoliated and CVD resonators. We found experimental indications that the dissipation of ALD MoS_2 membranes in heterostructures is roughly 3.7 times lower than that of purely exfoliated MoS_2 membranes, which is promising for high-performance 2D heterostructure resonators. Our results show possibilities toward exploiting ALD technique for nanomechancial resonators in explorations on atomically thin tunable resonators and 2D sensors. Further work could focus on the thickness control of ALD resonators, which can bring significant improvements in device performance and lead to new functionalities.

Methods

Sample fabrication

A Si wafer with 285 nm dry SiO_2 is spin coated with positive e-beam resist and exposed by electron-beam lithography. Afterwards, the SiO_2 layer without protection is completely etched using CHF_3 and Ar plasma in a reactive ion etcher. More details on the fabrication of substrate can be found in supplementary S1. The edges of cavities are examined to be well-defined by scanning electron microscopy and AFM (see figures S2(a) and (b)). After resist removal, few-layer graphene and ALD NbS_2 nanoflakes are exfoliated by Scotch tape, and then separately transferred onto the substrate at room temperature through a deterministic dry stamping technique.

Optothermal drive

We use an interferometer setup [26, 27] to measure the resonance frequency and Q factor of the fabricated resonators. An intensity-modulated blue laser ($\lambda = 405$ nm) irradiates the membrane resulting in a periodic heat flux to actuate it, while a intensity-fixed red laser ($\lambda = 633$ nm) is utilized to detect the motion. The heat flux results in a motion of the drum due to the thermal expansion force. All measurements are performed at room temperature inside a vacuum chamber at 10^{-6} mbar. A vector network analyzer (VNA) modulates the intensity of a blue laser at frequency ω to optothermally actuate a resonator while it analyzes the resulting intensity modulation of the red laser caused by the mechanical response of the same resonator. The red and blue laser powers used are 1.20 and 0.13 mW respectively, where the resonators vibrate in the linear regime and the temperature increase due to self-heating was negligible.

Data availability statement

All data that support the findings of this study are included within the article (and any supplementary files).

Acknowledgments

P G S and G J V acknowledge support by the Dutch 4TU federation for the Plantenna project. H L acknowledges the financial support from China Scholarship Council. H S J v d Z and P G S acknowledge funding from the European Union's Horizon 2020 research and innovation program under Grant Agreement Number 881603 (Graphene Flagship). S B B and A A B would like to acknowledge the European Research Council (Grant Agreement No. 648787-ALDofTDTMDs) for financial support. S B B acknowledges financial support from the Science for Diplomacy research program of the Dutch Research Council (NWO, Grant Number 483.20.029, 'Agricultural and environmental 2D gas sensors'). We thank Doon Hoon Shin for helping us with substrate fabrication.

Conflict of interest

The authors declare no competing financial or non-financial interests.

Author contributions

H L, S L, P G S and G J V conceived the experiments. H L performed the optomechanical measurements. H L and S L fabricated and inspected the samples. S B B and A A B synthesized and characterized ALD materials. H L, G J V and P G S analyzed and modeled the experimental data. H S J v d Z, A A B and P G S supervised the project. The paper was jointly written by all authors with a main contribution from H L. All authors discussed the results and commented on the paper.

ORCID iDs

Hanqing Liu https://orcid.org/0000-0002-3867-0160

Saurabh Lodha https://orcid.org/0000-0002-7581-6472
Peter G Steeneken https://orcid.org/0000-0002-5764-1218
Gerard J Verbiest https://orcid.org/0000-0002-1712-1234

References

[1] Barton R A, Ilic B, van der Zande A M, Whitney W S, McEuen P L, Parpia J M and Craighead H G 2011 High, size-dependent quality factor in an array of graphene mechanical resonators *Nano Lett.* **11** 1232–6
[2] Zhu J *et al* 2022 Frequency scaling, elastic transition and broad-range frequency tuning in WSe_2 nanomechanical resonators *Nano Lett.* **22** 5107–13
[3] Lee J, Wang Z, He K, Shan J and Feng P X-L 2013 High frequency MoS_2 nanomechanical resonators *ACS Nano* **7** 6086–91
[4] Steeneken P G, Dolleman R J, Davidovikj D, Alijani F and van der Zant H S J 2021 Dynamics of 2D material membranes *2D Mater.* **8** 042001
[5] Lemme M C *et al* 2020 Nanoelectromechanical sensors based on suspended 2D materials *Research* **2020** 8748602
[6] Ye F, Islam A, Zhang T and Feng P X-L 2021 Ultrawide frequency tuning of atomic layer van der Waals heterostructure electromechanical resonators *Nano Lett.* **21** 5508–15
[7] Mackus A, Bol A and Kessels W 2014 The use of atomic layer deposition in advanced nanopatterning *Nanoscale* **6** 10941–60
[8] Sharma A , Verheijen M A, Wu L, Karwal S, Vandalon V, Knoops H C M, Sundaram R S, Hofmann J P, Kessels W M M (E) and Bol A A 2018 Low-temperature plasma-enhanced atomic layer deposition of 2-D MoS_2: large area, thickness control and tuneable morphology *Nanoscale* **10** 8615–27
[9] Vos M F J, Macco B, Thissen N F W, Bol A A and Kessels W 2016 Atomic layer deposition of molybdenum oxide from $(N^tBu)_2(NMe_2)_2Mo$ and O_2 plasma *J. Vac. Sci. Technol.* A **34** 01A103
[10] Hao W, Marichy C and Journet C 2018 Atomic layer deposition of stable 2D materials *2D Mater.* **6** 012001
[11] Basuvalingam S B , Macco B, Knoops H C M, Melskens J, Kessels W M M (E) and Bol A A 2018 Comparison of thermal and plasma-enhanced atomic layer deposition of niobium oxide thin films *J. Vac. Sci. Technol.* A **36** 041503
[12] Castellanos-Gomez A , Poot M, Steele G A, van der Zant H S J, Agraït N and Rubio-Bollinger G 2012 Elastic properties of freely suspended MoS_2 nanosheets *Adv. Mater.* **24** 772–5
[13] Wang G , Dai Z, Xiao J, Feng S, Weng C, Liu L, Xu Z, Huang R and Zhang Z 2019 Bending of multilayer van der Waals materials *Phys. Rev. Lett.* **123** 116101
[14] Sheraz A , Mehmood N, Çiçek M M, Ergün İ, Rasouli H R, Durgun E and Kasırga T S 2021 High elasticity and strength of ultra-thin metallic transition metal dichalcogenides *Nanoscale Adv.* **3** 3894–9
[15] Sun H, Agrawal P and Singh C V 2021 A first-principles study of the relationship between modulus and ideal strength of single-layer, transition metal dichalcogenides *Mater. Adv.* **2** 6631–40
[16] Sun Y, Zhuo Z and Wu X 2018 Bipolar magnetism in a two-dimensional NbS_2 semiconductor with high Curie temperature *J. Mater. Chem.* **6** 11401–6
[17] Elder R M, Neupane M R and Chantawansri T L 2015 Stacking order dependent mechanical properties of graphene/MoS_2 bilayer and trilayer heterostructures *Appl. Phys. Lett.* **107** 073101
[18] Bertolazzi S, Brivio J and Kis A 2011 Stretching and breaking of ultrathin MoS_2 *ACS Nano* **5** 9703–9
[19] López-Polín G , Gómez-Navarro C, Parente V, Guinea F, Katsnelson M, Pérez-Murano F and Gómez-Herrero J 2015 Increasing the elastic modulus of graphene by controlled defect creation *Nat. Phys.* **11** 26–31
[20] Lee C, Wei X, Kysar J W and Hone J 2008 Measurement of the elastic properties and intrinsic strength of monolayer graphene *Science* **321** 385–8
[21] Ye F, Lee J and Feng P X-L 2017 Atomic layer MoS_2-graphene van der Waals heterostructure nanomechanical resonators *Nanoscale* **9** 18208–15
[22] Liu K *et al* 2014 Elastic properties of chemical-vapor-deposited monolayer MoS_2, WS_2 and their bilayer heterostructures *Nano Lett.* **14** 5097–103
[23] Šiškins M *et al* 2022 Nanomechanical probing and strain tuning of the Curie temperature in suspended $Cr_2Ge_2Te_6$-based heterostructures *npj 2D Mater. Appl.* **6** 1–8
[24] Aguila M A C, Esmenda J C, Wang J-Y, Lee T-H, Yang C-Y, Lin K-H, Chang-Liao K-S, Kafanov S, Pashkin Y A and Chen C-D 2022 Fabry–Perot interferometric calibration of van der Waals material-based nanomechanical resonators *Nanoscale Adv.* **4** 502–9
[25] Pezone R, Baglioni G, Sarro P M, Steeneken P G and Vollebregt S 2022 Sensitive transfer-free wafer-scale graphene microphones *ACS Appl. Mater. Interfaces* **14** 21705–12
[26] Liu H, Baglioni G, Constant C B, van der Zant H S J, Steeneken P G and Verbiest G J 2023 Enhanced photothermal response near the buckling bifurcation in 2D nanomechanical resonators (arXiv:2305.00712)
[27] Liu H, Lee M, Šiškins M, van der Zant H S J, Steeneken P G and Verbiest G J 2023 Tension tuning of sound and heat transport in graphene *Phys. Rev.* B **108** L081401